Journal Name

Cite this: DOI: 00.0000/xxxxxxxxxx

Supplementary information for Influence of near-surface oxide layers on TiFe hydrogenation: mechanistic insights and implications for hydrogen storage applications†

Archa Santhosh*,[a], ShinYoung Kang[b], Nathan Keilbart[b], Brandon C. Wood[b], Thomas Klassen[a], Paul Jerabek*,[a] and Martin Dornheim[a,1]

Contents

List of Figures

List of Tables

1 Computational details

A **k**-point folding factor of 1 was applied to the z-direction for all surface calculations. The surface formation energies (γ) were calculated with equation S1 where E_{slab} is the total energy of the slab, E_{bulk} is the total energy of the bulk structure, n is the number of bulk units in the surface slab and A_{slab} is the cross sectional area of the slab.
For asymmetric stoichiometric slabs, Ti- and Fe- terminations were created simultaneously upon cleavage. We relaxed the upper surface with each termination while constraining the lower layers to ensure a bulk like interior and calculated the surface energies using converged models with 14 bulk units.

$$\gamma = \frac{E_{slab} - nE_{bulk}}{2A_{slab}} \tag{S1}$$

The lowest energy structures for six oxygen coverages were predicted with a basin-hopping algorithm. A general sampling temperature (T) of 100 K was adopted which allowed minima search within $\approx$ 50 eV. Additional runs at higher temperatures (200 K, 300 K) were also carried out where necessary to escape the local minima before returning to the general temperature. A graph of the optimization process for 2 oxide layer thickness is plotted for 200 steps in Figure S1 as an example.

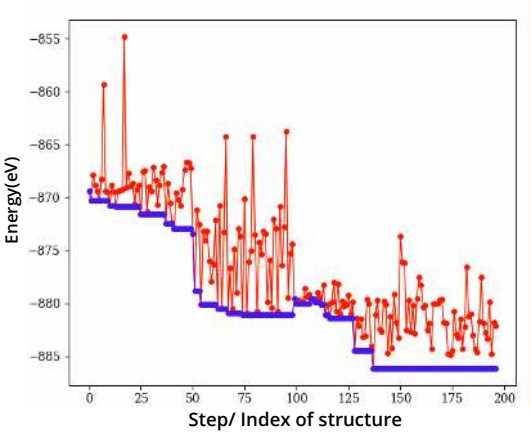

Figure S1 Basin-hopping global optimization steps for 2L-MO. The red dots are local minima obtained and blue lines are the basins.

For the generation of the surface phase diagram, surface energies with adsorbed H or O ($\gamma_{(\mathrm{ads})}$) were calculated with Equation S2, in which T is the temperature and R is the gas constant.[1]

$$\gamma_{(\mathrm{ads})} = \gamma_{(\mathrm{prist})} + (C \cdot (E_{\mathrm{slab}}^{\mathrm{ads},(T)} - RT \ln\left(\frac{p_{\mathrm{ads}}}{p^{\circ}}\right)) \tag{S2}$$

$$E_{\mathrm{slab}}^{\mathrm{ad},(T)} = E_{\mathrm{slab+adatom}} - (E_{\mathrm{prist}} + NE_{\mathrm{adatom}}^{(T)})/N \tag{S3}$$

$$E_{\mathrm{adatom}}^{(T)} = E_{\mathrm{adatom}}^{(0K)} - TS^{(T)} \tag{S4}$$

$\gamma_{(\mathrm{prist})}$: Surface energy of the pristine surface
p°:Reference pressure (1 bar)
p_{ad}: Partial pressure of the adsorbent species
C: Coverage after adsorption
$E_{\mathrm{slab+adatom}}$: Total energy of the slab with adsorbed species
N: Number of adsorbed species
$S^{(T)}$: Entropy of the gaseous adsorbent in standard state

2 TiFe surface

2.1 Low energy surfaces of TiFe

The equilibrium crystal shape (Wulff shape) of TiFe IMC is calculated from the surface formation energies with pymatgen.[2]

The obtained Wulff shape is shown in Figure S2.
Table S1 contains γ (in J/m^2) and area fractions (%) of relevant surfaces.

Table S1 TiFe surface formation energies(γ) in J/m^2 and the percentage area fractions of respective surfaces.

(hkl)	(100)	(110)	(111)	(211)	(310)	(321)
γ	2.686[a] 2.610[b]	2.095	2.306[a] 2.486[b]	2.306	2.390	2.275
(%)	0.00	57.17	0.85	6.00	13.82	22.15

[a] Ti-terminated surface [b] Fe-terminated surface

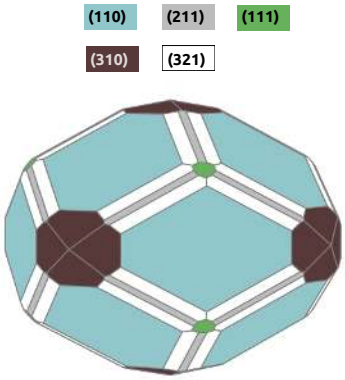

Figure S2 The equilibrium crystal shape of TiFe IMC. The radius of the particle is 2.277 Å.

2.2 TiFe (110) surface sites

The nine surface sites identified are given in Fig S3. The light green triangles represent the four different m_i-m_i-m_j threefold sites, red dashed lines represent the three m_i-m_j bridge sites and blue dotted circles the metal on-top sites.

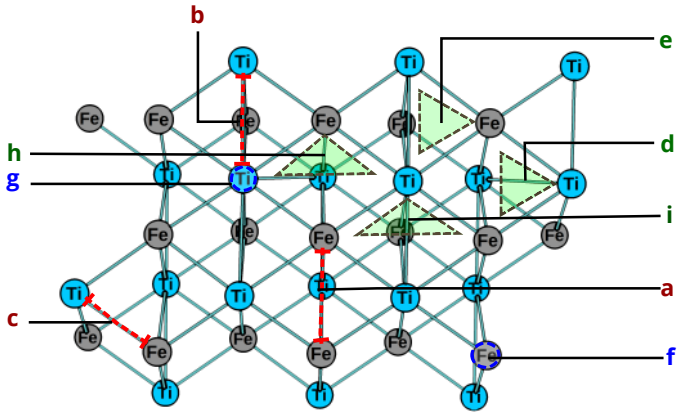

Figure S3 The sites identified at the TiFe (110) surface. a) Fe-Fe bridge, b) Ti-Ti bridge, c) Ti-Fe bridge, d) Fe-Fe-Ti threefold site, e) Ti-Ti-Fe threefold site, f) Fe on-top site, g) Ti on-top site, h) Ti-Ti-Fe threefold site, i) Fe-Fe-Ti threefold site. (Top view of the surface)

2.3 Oxide layer growth on TiFe (110) surface

The side view of the oxide layer growth at 1L, 2L and 3L thickness are given in Fig S4. Considerable clustering can be observed as the O content is increased to the 3L-MO. The cavities present may aid H penetration or oxide removal on a later stage.

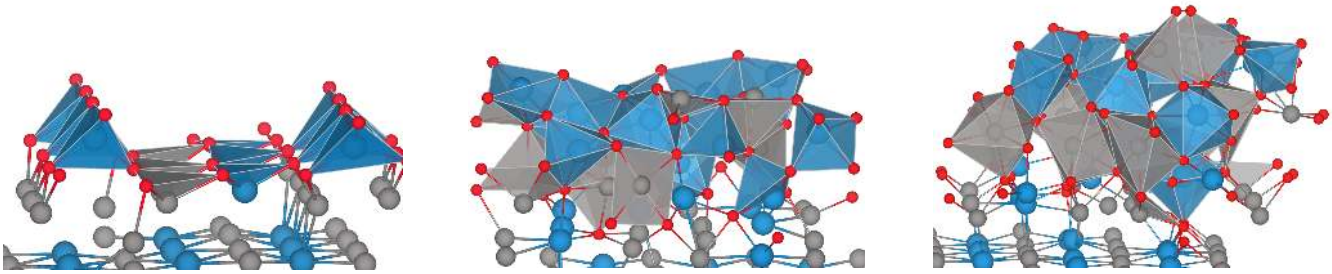

(a) 1L-MO **(b)** 2L-MO **(c)** 3L-MO

Figure S4 Oxide-layer growth on the TiFe(110) surface at increasing coverages(Side view). Blue, grey and red balls represent Ti, Fe and O respectively.

2.4 Atomic charge analysis

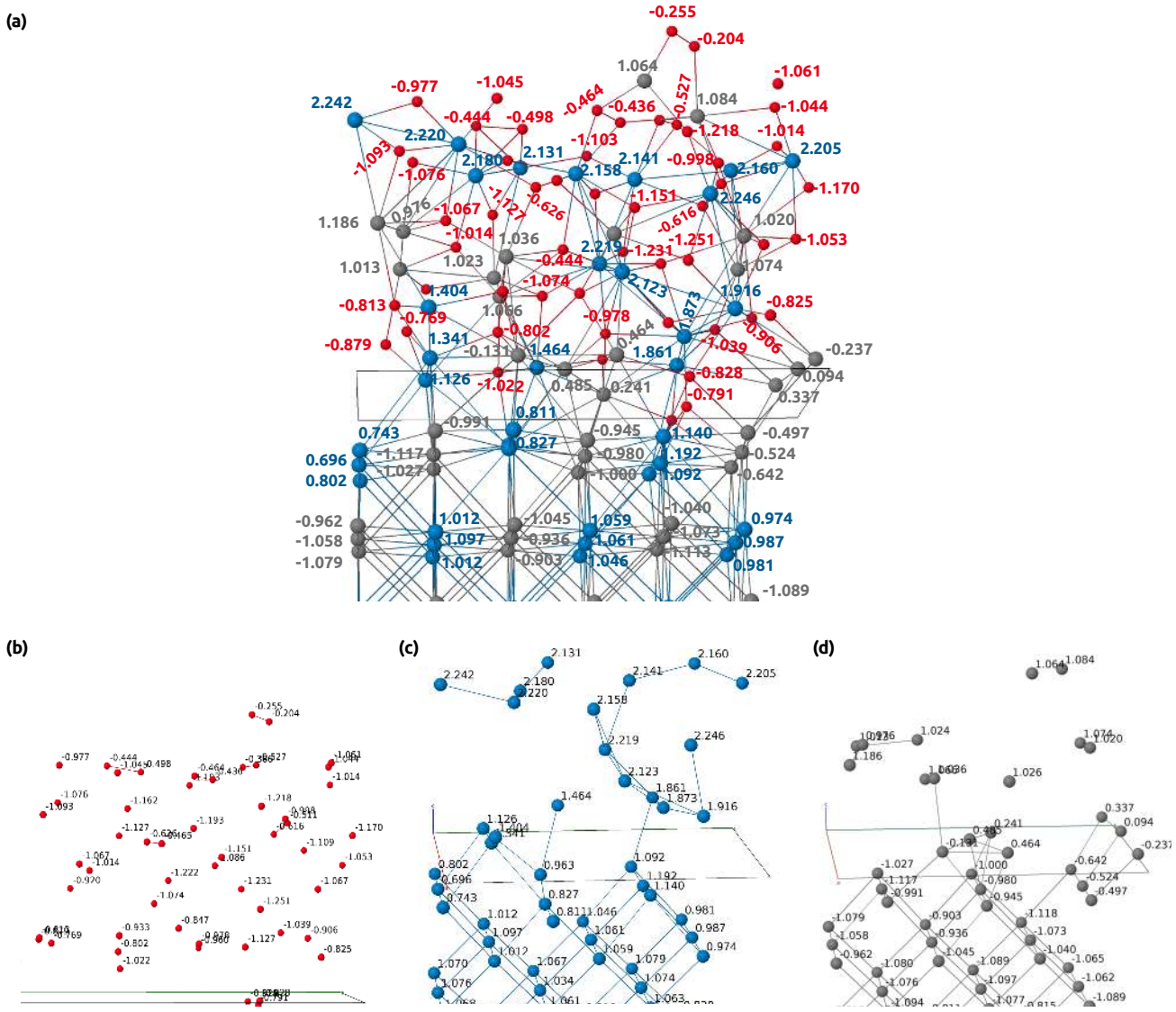

Figure S5 Net atomic charges (NAC) on the 3L-MO system. (a) Side-view with NAC labelled on all visible sites (Blue, grey and red corresponds to Ti, Fe and O, respectively). (b), (c) and (d) shows the NAC extracted for O, Ti and Fe respectively

3 Hydrogenation energetics of the oxidized TiFe surface

Hydrogen molecule dissociation and adsorption on the fully oxidized surface (3L-MO) was studied at the surface exposed O, Ti, and Fe sites. Dissociation at a surface Ti site takes an activation energy E_{act} of 1.933 eV. In addition, a high energy barrier of 2.028 is also observed for H_2 dissociation and adsorption on the same O atom. Their minimum energy paths (MEP) along with the initial and final states are plotted in Fig S6.

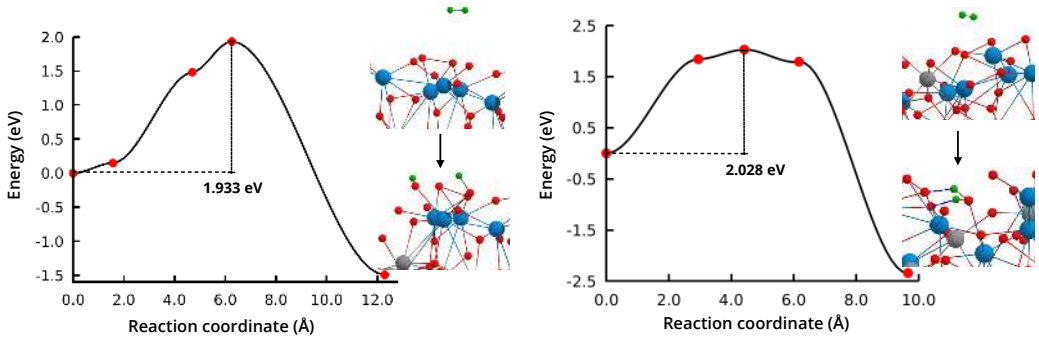

(a) H_2 dissociation on top of an exposed Ti

(b) H_2 dissociation on top of a surface O

Figure S6 H_2 dissociation and adsorption at two different surface exposed sites on the 3L-MO surface. The initial and final configurations are given along side the respective minimum energy paths.

3.1 Hydrogen migration

Hydrogen binding energies at different sites from the top of the oxidized surface (T1) to the bulk interface region (T5) is given in Table S2.

Table S2 Binding energies of H at different sites at levels labelled as T1 to T5 from top of the oxide layer to the bulk interface region. Six lowest energies are listed at each level.

Site level	Binding energy (eV/H)
T1	−2.8829, −1.6715, −1.4825, −1.4518, −1.4359, −1.1252
T2	−1.2756, −1.0773, −0.9508, −0.8720, −0.8264, −0.7753
T3	−0.7047, −0.4180, −0.1643, −0.1629, 0.0734, 0.0898
T4	−0.8348, −0.1336, 0.1836, 0.7893, 0.7895, 1.2473
T5	−0.7500, −0.6640, −0.6615, −0.5971, −0.5199, −0.3731

Hydrogen migration to the T5 region in the presence of already adsorbed H atoms were studied starting from an optimized 3L-MO:9H model. One H atom was added randomly at varying oxide-layer depths and based on the energetics of 3L-MO:10H, possible migration paths were assessed. Figure S7 shows the CI-NEB plots for hydrogen diffusion **Path 3** for a H atom to reach the near bulk-interface region in 3L-MO:10H system.

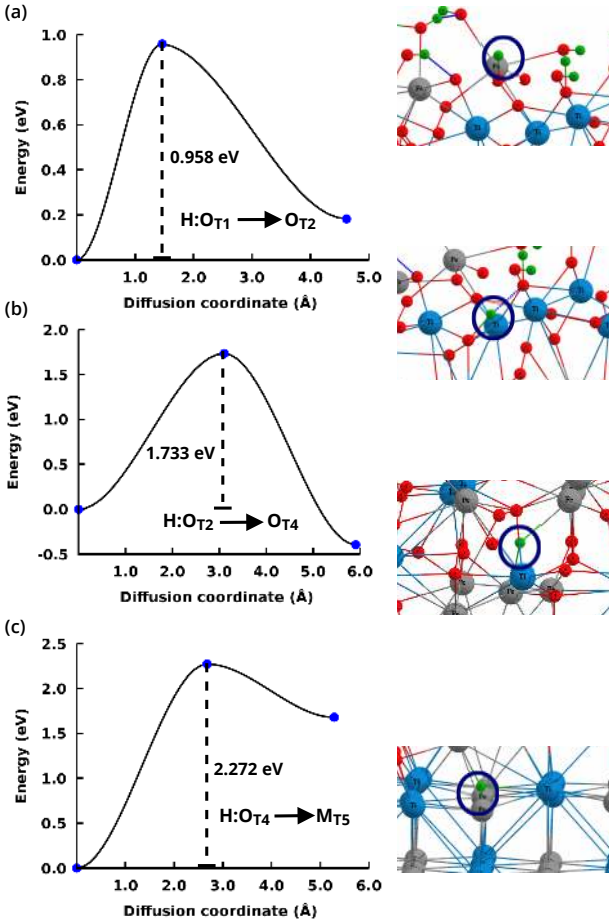

Figure S7 Hydrogen diffusion at increased H content in oxide layer using the 3L-MO:10H system (Path **3** in Table 3). The initial and final structures are given alongside the plots.

4 *Ab-initio* molecular dynamics (AIMD)

Six excess O_2 molecules were allowed to react with the 3L-MO model and the simulation progress was followed. Figure S8 shows snapshots of this model taken at different points in the AIMD run. It can be seen that some of the excess oxygen only weakly attach to the top-most layer without dissociation into atomic oxygen.

The snapshots of end structures for 1L to 3L coverages after AIMD simulations at 600 K for a period of 10 ps are given in Fig S9. Smooth Overlap of Atomic Positions (SOAP) descriptors [3–7] were employed to identify the crystalline structural matches for the amorphous oxide layers on the oxide layer models. The results are summarized in Table S3.

4.1 Radial distribution function

The radial distribution function (RDF) for the 1L-MO, 2L-MO, 3L-MO and the excess-O_2 models are plotted in Fig S10.

Interaction of hydrogen with the 3L-MO system is investigated at different temperatures with the 3L-MO:28H model and a summary of the bond lengths and bond angles after a simulation period of 10 ps is given in Table S4.

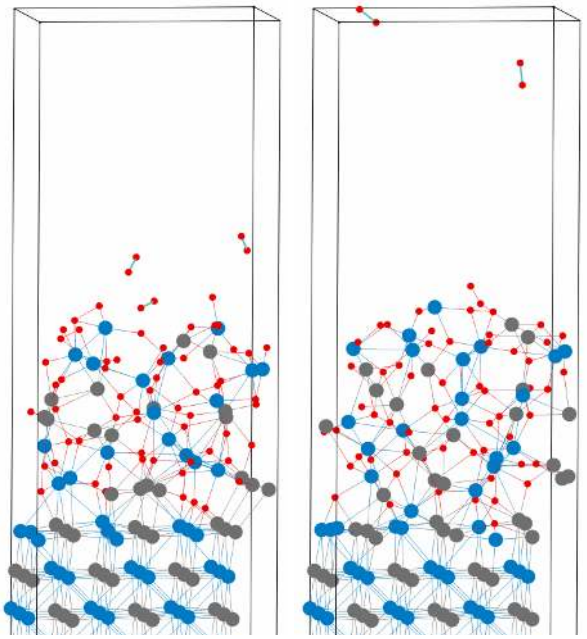

(a) 0.5 ps **(b)** 5 ps

Figure S8 AIMD snapshots of the 3L-MO structure with six excess O_2 molecules performed at 673 K after 0.5 ps (left) and 5 ps (right).

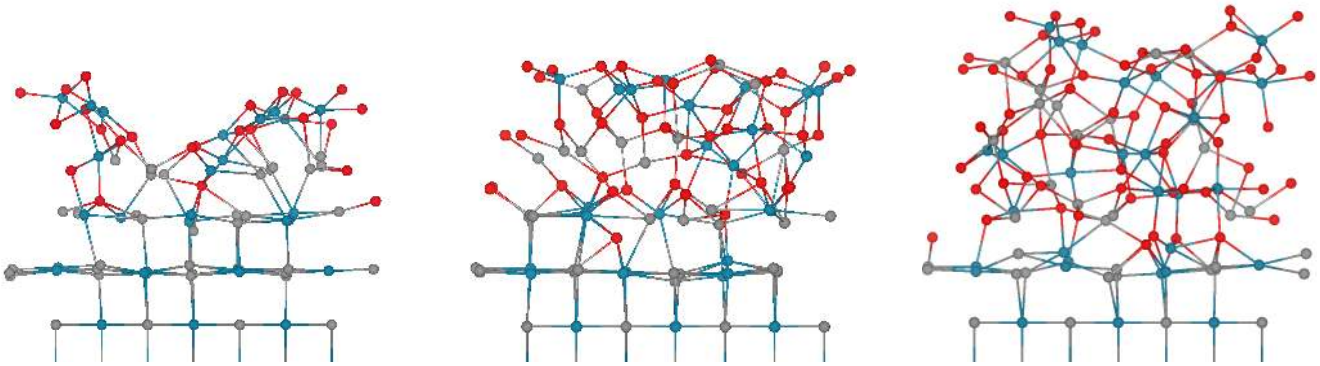

(a) 1L-MO: 600 K, 10 ps **(b)** 2L-MO: 600 K, 10 ps **(c)** 3L-MO: 600 K, 10 ps

Figure S9 AIMD end structures for 1L, 2L and 3L coverages at 600 K.

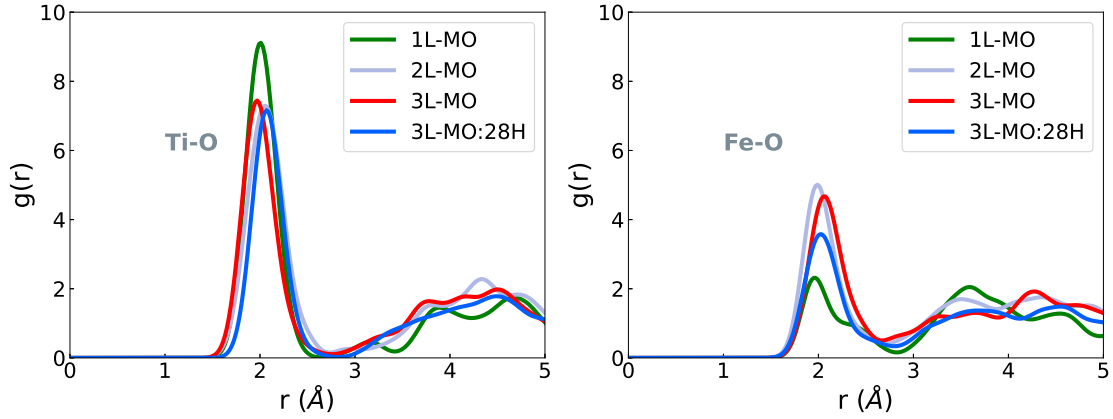

(a) Ti-O 600K, 10 ps end structure **(b)** Fe-O 600K, 10 ps end structure

Figure S10 Radial distribution functions of the oxidized surface at 600 K after a simulation period of 10 ps for different surface oxide models.

Table S3 Structural matches identified for the oxide films with SOAP descriptors for the oxide layer models (1L-, 2L- and 3L-MO) at different AIMD simulation temperatures. For 3L-MO, the hydrogenated structure (3L-MO:28H) was included. The value of structural similarity is given in parenthesis.

Model	Structural matches
1L-MO : 600 K	$Ti(FeO_2)_2$(0.7957), $TiFeO_3$(0.7702), $Ti_2Fe_4O_9$* (0.7665), $Ti(FeO_2)_3$(0.7661)*, Ti_2FeO_5(0.7445), $TiFe_2O_5$(0.7410), .., TiO* (0.6841), TiO_2(0.6832) .., FeO (0.6830), Fe_2O_3 (0.6816)
1L-MO : 300 K	$Ti(FeO_2)_2$(0.8837), $TiFeO_3$(0.8583), $Ti_2Fe_4O_9$*(0.8542), $TiFe_2O_5$(0.8285), Ti_2FeO_5(0.8125)
2L-MO : 600 K	$Ti(FeO_2)_2$(0.8203), $TiFeO_3$(0.7939), $Ti_2Fe_4O_9$*(0.7915), $Ti(FeO_2)_3$(0.7898)*, Ti_2FeO_5(0.7675), $TiFe_2O_5$ (0.7663), .., TiO* (0.6940), TiO_2(0.6936), Ti_3O_5(0.6934), .., FeO(0.6936), Fe_3O_4 (0.6935)
2L-MO : 300 K	$Ti(FeO_2)_2$(0.8201), $TiFeO_3$(0.7936),$Ti_2Fe_4O_9$*(0.7913), $TiFe_2O_5$(0.7677), Ti_2FeO_5(0.7661)
3L-MO : 600 K	$TiFeO_3$(0.8949), $Ti(FeO_2)_2$(0.8866), $Ti_2Fe_4O_9$*(0.8768), Ti_2FeO_5(0.8684), $TiFe_2O_5$ (0.8665), $TiFeO_4$*(0.8254), .., Ti_2O_3(0.7457), TiO_2(0.7451), .., Fe_2O_3(0.7428), Fe_3O_4(0.7426),
3L-MO : 750 K	$TiFeO_3$ (0.9470), $Ti(FeO_2)_2$(0.9133), $Ti_2Fe_4O_9$*(0.9037), Ti_2FeO_5(0.8962), $TiFe_2O_5$(0.8948)
3L-MO : 28H, 600 K	$FeHO_2$(0.7907), $Ti_2H_2O_3$*(0.7910), $Fe(OH)_2$(0.7886), $Ti(HO)_2$*(0.7858), $TiFeO_3$(0.7840), $Ti_3H_2O_7$*(0.7628), $Ti(FeO_2)_2$*(0.7296), $TiFeO_4$*(0.7192), $Ti_2Fe_4O_9$ (0.7294), Ti_2FeO_5(0.7117), $TiFe_2O_5$(0.7117)

**Unstable configuration*

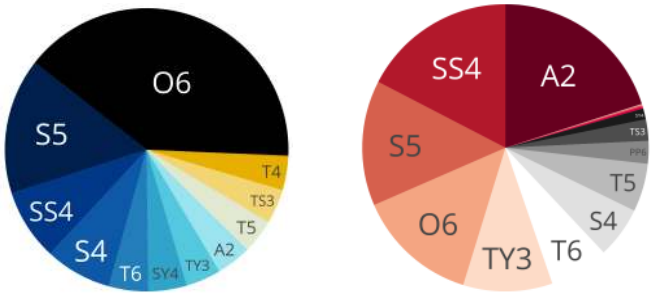

(a) Ti-coordinations **(b)** Fe-coordinations

Figure S11 Fractions of metal (Ti/Fe)-O-H coordination environments present in the hydrogen adsorbed system (3L-MO:28H) at 600 K.

Table S4 Bond distances (d) and bond angles (A) between O and H at different temperatures after an AIMD run of 10 ps. 0 K results corresponds to that of the DFT optimized structure.

Model	T(K)	d_{O-H} (Å)			A_{H-O-H} (°)		
		Min	Max	Mean	Min	Max	Mean
3L-MO:28H	0K	0.9728	1.0450	1.0025	104.59	105.82	105.21
	300K	0.9462	1.0464	0.9962	100.94	115.78	107.32
	600K	0.9354	1.0476	0.9948	100.33	108.29	104.27
	750K	0.9123	1.0430	0.9764	99.58	110.61	104.63

Notes and references

[1] K. Reuter and M. Scheffler, *Phys. Rev. B*, 2002, **65**, 035406.

[2] S. P. Ong, W. D. Richards, A. Jain, G. Hautier, M. Kocher, S. Cholia, D. Gunter, V. L. Chevrier, K. A. Persson and G. Ceder, *Comput. Mater. Sci.*, 2013, **68**, 314–319.

[3] A. P. Bartók, R. Kondor and G. Csányi, *Phys. Rev. B*, 2013, **87**, 184115.

[4] A. P. Bartók, R. Kondor and G. Csányi, *Phys. Rev. B*, 2013, **87**, 219902.

[5] A. P. Bartók, R. Kondor and G. Csányi, *Phys. Rev. B*, 2017, **96**, 019902.

[6] L. Himanen, M. O. Jäger, E. V. Morooka, F. Federici Canova, Y. S. Ranawat, D. Z. Gao, P. Rinke and A. S. Foster, *Comput. Phys. Commun.*, 2020, **247**, 106949.

[7] S. De, A. P. Bartók, G. Csányi and M. Ceriotti, *Phys. Chem. Chem. Phys.*, 2016, **18**, 13754–13769.